AIAA JOURNAL
Vol. 48, No. 3, March 2010

Three-Dimensional Analysis of a Supersonic Combustor Coupled to Innovative Inward-Turning Inlets

Faure J. Malo-Molina* and Datta V. Gaitonde†
U.S. Air Force Research Laboratory, Wright–Patterson Air Force Base, Ohio 45433
Houshang B. Ebrahimi‡
Flow Modeling and Simulation, LLC, Carson City, Nevada 89701
and
Stephen M. Ruffin§
Georgia Institute of Technology, Atlanta, Georgia 30332

DOI: 10.2514/1.43646

Three-dimensional simulations are employed to examine the effect of inlet distortion and model fidelity with Reynolds averaged Navier–Stokes or large eddy simulation approaches for a generic circular cross-sectional supersonic combustor at a flight condition of Mach 6 and an altitude of about 24.2 km. To examine inlet distortion effects on combustion, frozen and finite rate chemistry simulations are performed on combustors connected to two different types of streamline-traced inlets (denoted "Scoop" and "Jaws") with the Wilcox k–ω turbulence model. For comparison, uniform inflow boundary condition to the combustor is also simulated. The metrics employed include qualitative assessments related to flow structure as well as quantitative values of fuel combustion efficiency and thrust ratios. The results indicate a complex overall effect of distortion due to inlet design. For Jaws, the increased pressure loss associated with distortion is mitigated slightly by improved combustion efficiency and better thrust performance. The Scoop inlet has lower distortion and better recovery, but the combustion coefficient is lower than Jaws. In the second part of this study, finite rate chemistry results with unsteady Reynolds averaged Navier–Stokes are compared with those from large eddy simulation with an uniform inflow profile. Differences in transient processes include the manner in which large- and small-scale structures originate and evolve in the cavity recirculation and downstream regions. The finer details observed with the large eddy simulation model have significant consequences on the overall field, including the unsteady position of the shock structure arising from the interaction of the incoming flow with the cavity shear layer, combustion processes, and injection jet interactions.

I. Introduction

HYPERSONIC air-breathing flight will enable rapid transport as well as affordable access to space (see, e.g., [1]). Despite advances in high-speed propulsion analysis, adequate sustained thrust at hypersonic speeds remains difficult to achieve. Some of the main difficulties can be traced to aeropropulsive phenomena, including transition to turbulence, shock–boundary-layer interactions, fuel injection and mixing in a short residence time environment, and their collective impact on heat load, inlet distortion, and adequate thrust generation in a practical engine.

Recent advances have employed a spectrum of loosely coupled approaches, including flight tests (e.g., [2]), analytical (e.g., [3]), and simulation (e.g., [4–8]). Each approach has inherent strengths and limitations. For example, in the computational approach, which is the focus of this paper, the availability of 3-D unsteady data greatly facilitates interrogation and trend detection. However, the multiphysics nature of the phenomena introduces significant difficulties. In addition to traditional verification issues associated with grid and time-step-size spacing, the accuracy of chemical kinetics and assumptions invoked in turbulence modeling are major sources of uncertainties. The thrust of this paper is twofold. In the first part, simulations are employed to explore the effect of inlet distortion for discovery purposes, whereas, in the second part, the effect of modeling fidelity is discussed.

The effect of inlet distortion on the combustion process downstream is examined in the context of two inlet designs depicted in Figs. 1a and 1b. The Jaws inlet (Fig. 1a) consists of streamline-traced surfaces to ensure planar shocks. This inlet has the potential to mitigate some of the principal issues encountered in more conventional configurations, including high thermomechanical loads produced by cowl lip interactions, flow spillage, and distortions created by flow separation and vortices [9]. The Scoop inlet (Fig. 1b) is a Busemann inlet design. The surface is traced with streamlines envisioned as solid surfaces, allowing the generation of inlets with swept walls. These swept surfaces provide a mechanism for flow spillage, which enlarges the self-starting envelope of the inlet [10]. Both inlets are designed for equal flight conditions (Mach 6, dynamic pressure of 71.82 kPa) with the same contraction ratio and end in circular cross sections, thus facilitating the common combustor design described later [11].

Despite careful design, however, all practical inlets generate flowfield distortions through complex shock–boundary-layer interactions. Although these interactions result in increased losses and potentially adversely impact isolator performance, they can also engender a region of enhanced turbulence in the isolator, yielding better mixing of air and fuel and, thus, potentially augmenting chemical reactions and overall efficiency of the system [12]. Thus, two principal issues that must be examined are 1) the three-dimensional interplay between viscous and inviscid interactions including shock–boundary-layer and shock–shock interactions in the inlet, and 2) the effects of these interacting with a jet and the combustion of the reacting fuel–air mixture [13–15].

The common combustor design for both inlet configurations uses an open cavity with a length-to-depth ratio of 4. The cavity is the circular equivalent of the rectangular variant commonly employed, the principal flow features of which are shown in Fig. 2. The objective

Presented as Paper 131 at the 47th AIAA Aerospace Sciences Meeting Including the New Horizons Forum and Aerospace Exposition, Orlando, FL, ; received 5 February 2009; revision received 31 August 2009; accepted for publication 10 September 2009.

*Research Engineer, Air Vehicles Directorate. Member AIAA.
†Technical Area Leader, Air Vehicles Directorate. Fellow AIAA.
‡Scientist. Associate Fellow AIAA.
§Associate Professor. Member AIAA.

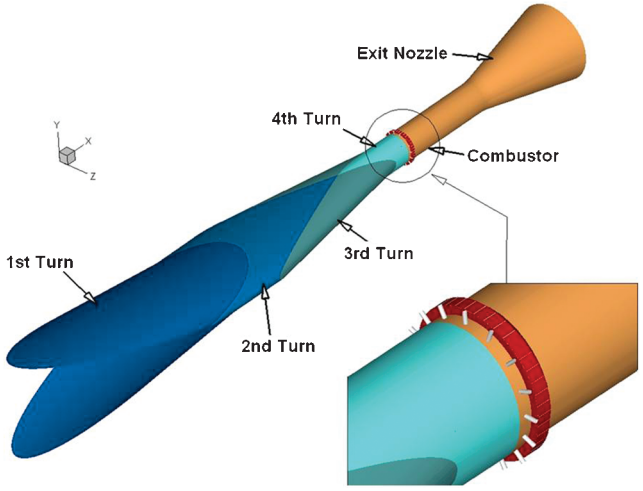

a) Jaws

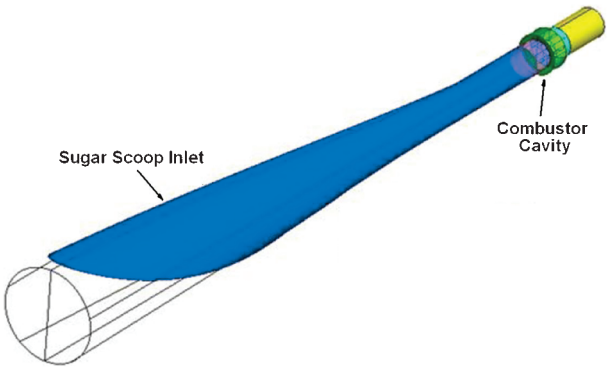

b) Scoop

Fig. 1 Nonrectangular hypersonic inlet configurations coupled to circular combustors.

of the cavity is to help initiate and maintain stable combustion in an efficient fashion. The large subsonic region generated by the cavity alleviates problems arising from the short residence time and enhances mixing [16–20]. Because the drag from flow separation is much less over a cavity than a bluff body, a cavity within the combustor region provides a stable flame holder and relatively small total pressure losses. In this open cavity configuration, the rear wall is angled and serves to suppress the unsteady nature of the free shear layer [21–23]. The injector arrangement, described in greater detail later, is based on parametric results with the rectangular as well as circular configurations [18,24]. In examining inlet distortion effects, the Reynolds averaged Navier–Stokes (RANS) approach with the k–ω model is employed [25]. Both nonreacting and reacting conditions are considered and, for comparison purposes, an average uniform inflow is also investigated as a baseline. The entrance condition to the combustor is the mean steady inlet exit, distorted or uniform profile. It is assumed that the device is boosted to cruise conditions by other means.

The RANS approach is adopted almost exclusively for engineering analyses because of the lower computational requirements. RANS simulations provide a measure of qualitative insight into the various processes, in addition to trend data for parametric studies, with a closure model based on semi-empirical considerations that is calibrated for relatively simple situations. The technique must thus be evaluated carefully for each new situation. An understanding of the physics must, however, resolve the fundamentally unsteady interactions, including large regions of subsonic flow within the cavity, shock–shock and shock–boundary-layer interactions, separated flow regions, nonequilibrium transfer of turbulence energy, and interactions between turbulence and chemical kinetics. The large eddy simulation (LES) method is generally considered to yield higher-fidelity results, because, in addition to a fundamentally different filtering process, larger scales are resolved if the mesh is adequate while closure modeling assumptions are invoked on a finer (subgrid) scale, where some semblance of isotropy may be more appropriate. Unlike typical steady-state turbulence models, the subgrid models for LES are a function of the local grid (or filter) size. Advanced combustion models in this category have been described and employed in [7,26,27]. Even with the availability of very large parallel processing systems, the significantly higher computational expense must, however, be factored in for each problem. To evaluate the effect of the computational model, in the second part of this study, the unsteady RANS (URANS) approach is compared with results from LES for the transient flow established when fuel injection is initiated. For this case, the inflow to the combustor is assumed to be uniform.

The paper is structured as follows. Section II outlines the theoretical and numerical model, delegating details to previous publications. The results in Sec. III are divided into Secs. III.A and III.B describing, respectively, the effect of inlet distortion and model fidelity. Section III.A is further divided into a description of the inlet distortion pattern with both Scoop and Jaws designs (Sec. III.A.1), the rationale for the fuel injection strategy in the combustor (Sec. III.A.2), and combustor performance with frozen (Sec. III.A.3) and finite rate (Sec. III.A.4) chemistry.

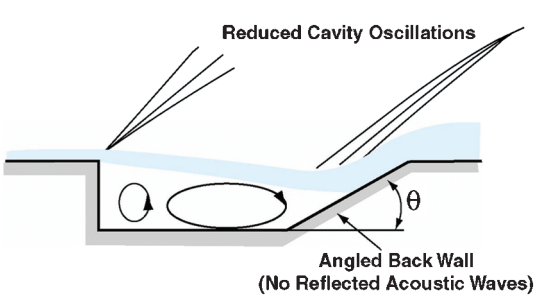

Fig. 2 Flowfield schematic in open cavity.

II. Theoretical and Computational Model

Complex phenomena typically encountered in supersonic combustion include large regions of subsonic flow, shock–shock and shock–boundary-layer interactions, separated flow, complex mixing processes, nonequilibrium transfer of turbulence energy, and interactions between turbulence and chemical kinetics. The code employed in this work is HEAT-3D, a more advanced version of GPACT. The code has previously been successfully applied to a variety of supersonic and subsonic combustion problems. Extensive validation for fully coupled, three-dimensional flows with finite rate chemistry has been reported in several previous studies [13,28,29].

The RANS and URANS models require specification of the eddy viscosity for closure. For this, the k–ω variant described in [25] is used together with laminar conservation species equations. For LES, the general conservation equations for mass, momentum, energy, and chemical species are filtered to obtain equations for the large (energy containing) scales. The unknown terms arising from the closure problem appear as subgrid terms, which are detailed in [26] and which must be modeled. Here the subgrid turbulence is approximated with the localized dynamic kinetic-energy model (LDKM) [26]. The eddy viscosity is computed as a function of the local grid size (Δ) and the subgrid turbulent kinetic energy (k_{SGS}): $\nu_t = C_t \Delta k_{SGS}^{0.5}$. A transport equation for k_{SGS} is solved requiring terms that are obtained from velocity gradients at a test filter level. The test filter width is taken to be twice the grid filter width. The subgrid chemistry is described with an assumed probability density function (PDF), which is a two-dimensional function of the species fraction and progress variable (change of the fuel mass fraction over time). These variables are assumed to be independent of each other. Filtered transport equations for the mean and variance of the mixture fraction and reaction progress are solved. The subgrid reaction rate is obtained by integrating the instantaneous fuel reaction rate over the 2-D PDF. Source terms in the transport equations for the mixture fraction and progress variable variance are obtained from the subgrid turbulent kinetic energy and dissipation rate (see [6,26]). Currently,

Table 1 Chemical mechanism for ethene–air mixture

Reaction 1	$C_2H_4 \leftrightarrow C_2H_2 + H_2$	Reaction 11	$H + OH + M \leftrightarrow H_2O + M$
Reaction 2	$C_2H_2 + O_2 \leftrightarrow 2CO + H_2$	Reaction 12	$H + O + M \leftrightarrow OH + M$
Reaction 3	$CO + O + M \leftrightarrow CO_2 + M$	Reaction 13	$2O + M \leftrightarrow O_2 + M$
Reaction 4	$CO + O_2 \leftrightarrow CO_2 + O$	Reaction 14	$N + NO \leftrightarrow N_2 + O$
Reaction 5	$CO + OH \leftrightarrow CO_2 + H$	Reaction 15	$N + O_2 \leftrightarrow NO + O$
Reaction 6	$OH + H_2 \leftrightarrow H_2O + H$	Reaction 16	$N + OH \leftrightarrow NO + H$
Reaction 7	$O + OH \leftrightarrow O_2 + H$	Reaction 17	$H_2 + O_2 \leftrightarrow 2OH$
Reaction 8	$O + H_2 \leftrightarrow OH + H$	Reaction 18	$2H + H_2 \leftrightarrow 2H_2$
Reaction 9	$2OH \leftrightarrow O + H_2O$	Reaction 19	$2H + H_2O \leftrightarrow H_2 + H_2O$
Reaction10	$2H + M \leftrightarrow H_2 + M$	Reaction 20	$2H + CO_2 \leftrightarrow H_2 + CO_2$

the HEAT-3D code is limited to the LDKM model, but others will be employed in the future. The PDF method is similar to the filtered density function method, which is considered a general success in simulating turbulent combustion (see [30–33]). This method has been used in many situations to account for the effect of chemical reactions in an exact manner regardless of the speed of the reaction (such as flameless regimes and distributed reaction zones).

Both URANS and LES computations share other aspects of HEAT-3D, including fully implicit time integration and strongly conservative finite volume formulation. Combustion is modeled using a finite rate, ethene chemistry model and Gordon/McBride thermodynamic curve fits. Thirteen gaseous chemical species are considered ($C_2H_4, C_2H_2, CO_2, CO, OH, O_2, O, H_2, H, H_2O, NO, N$, and N_2) with 20 chemical reactions representing a reduced reaction mechanism for reactants and products for ethene fuel and air oxidizer (see Table 1). The reduced mechanism, using the coefficients provided in [34], has been validated against experimental data on premixed cases.

Structured body conforming meshes are employed with emphasis on ease of generation. For the inlet distortion effect analysis, because no angle of attack or sideslip is considered in this paper (see [9] for results at off-design conditions), the Jaws simulation considers one-quarter of the azimuthal direction (because it has both horizontal and vertical symmetry) whereas Scoop, which has only a vertical plane of symmetry, considers one-half of the configuration. The Scoop configuration employs roughly 8×10^6 points, whereas Jaws has 4×10^6. The mesh is clustered toward the outer walls and around the injectors to capture the proper flow physics. In the equilibrium boundary layer just upstream of the first shock interaction, a y^+ of less than one is obtained. Additional grid details may be found in [11].

In the second part of the study, URANS and LES calculations are compared on a domain restricted to a one-eigth sector of the circumference, as shown in Fig. 3. The computational grid consists of 7.8×10^6 grid points distributed to resolve the flow in the cavity and around the fuel injector. The volume of the average grid size cell is about 5×10^{-11} m^3, with mean x and r spacings of 4×10^{-4} and 1×10^{-4} m, respectively. The time-step size is fixed at 1×10^{-6} s. Symmetry boundary conditions are enforced at the azimuthal boundaries and a fixed uniform inflow condition is specified with primitive variables, as described in Sec. III.A. This corresponds to $M_{\text{air}} = 2.2$, $T_s = 960$ K, and $\rho_{\text{air}} = 0.260$ kg/m^3 (no boundary layer was assumed). For all cases, fuel injection conditions correspond to $\rho_{\text{fuel}} = 2.90$ kg/m^3 and $U_{\text{fuel}} = 400$ m/s. The combustor and injector walls are modeled with a no-slip, adiabatic boundary condition. The outflow supersonic boundary condition is modeled using first-order extrapolation. Both unsteady approaches (URANS and LES) were initialized in the same manner with steady-state solutions without injection. Subsequently, fuel was injected at 300 K, whereas, for ignition, the Arrhenius reaction rate was calculated at 1200 K for the first 1000 iterations and subsequently reset to the proper values once reactions were initiated.

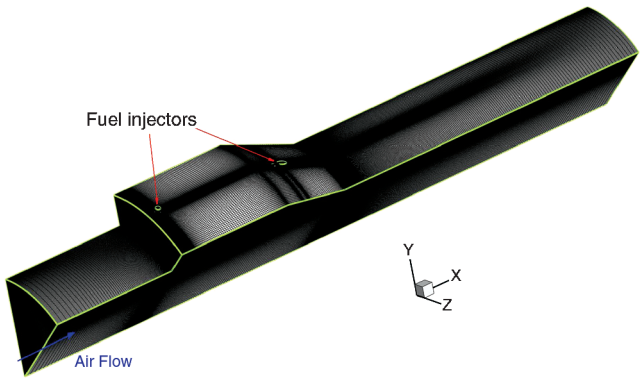

Fig. 3 Computational grid for LES and URANS.

III. Results

Several calculations are now presented with the goal of examining the effect of distortion and model fidelity. These are classified in Table 2. Cases 1a and 1b correspond to a uniform inflow, with 1a being the frozen case and 1b being the finite rate reacting case. Similarly, cases 2a and 2b represent the Jaws case, whereas cases 3a and 3b are the corresponding Scoop cases. Cases 4 and 5 employ URANS and LES, respectively, with finite rate chemistry.

A. Effect of Flow Distortion on Combustion

1. *Flow Distortion Because of Inlet*

Details of the distortion generated by Jaws and Scoop inlets are described first, to set the stage for subsequent discussion. Figures 4a and 4b depict the Mach number contours in the symmetry plane and several crossflow stations, including the exit plane for each inlet. The Jaws inlet generates planar shocks at the leading edges (despite its curved surfaces) analogous to the rectangular configuration [11]. At the downstream (exit of the inlet) plane, the Jaws profile exhibits two regions of low Mach number (top and bottom surfaces, respectively; see Fig. 4a). Previous analysis [11] has shown that these are generated by the swept shock–boundary-layer interaction similar to that observed in the double-fin configuration [35]. Essentially, the incoming boundary layer on the inlet wall separates and fluid from the sides is entrained to yield a mushroomlike feature. The Scoop profile, on the other hand, is generated by a sequence of conical shocks, yielding a relatively more uniform flow with a lower Mach

Table 2 Cases computed

Cases	Inflow	Time accuracy	Chemistry
1a/b	Uniform	Steady	a) Frozen / b) finite rate
2a/b	Jaws	Steady	a) Frozen / b) finite rate
3a/b	Scoop	Steady	a) Frozen / b) finite rate
4	Uniform	Unsteady (RANS)	Finite rate
5	Uniform	Unsteady (LES)	Finite -rate

Table 3 Exit/inlet force ratio and combustion efficiency for cases 1–3b

Inlet profile	F_e/F_i	Combustion efficiency %
Uniform	2.23	64
Jaws	2.63	67
Scoop	2.22	63

region in the upper part of the plane. (Note that when inserted as an upstream condition to the combustor, the profile has been reflected about the horizontal symmetry plane. Thus, in subsequent figures, such as Fig. 4b, the higher Mach number region is on the upper side.) These exit plane profiles are imposed as the inflow condition for the circular cross-sectional combustor, as described next.

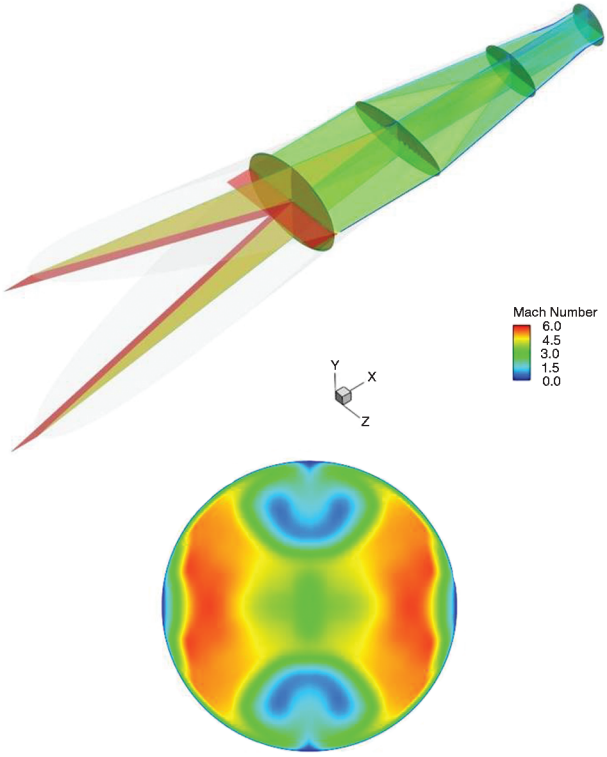

a) Jaws

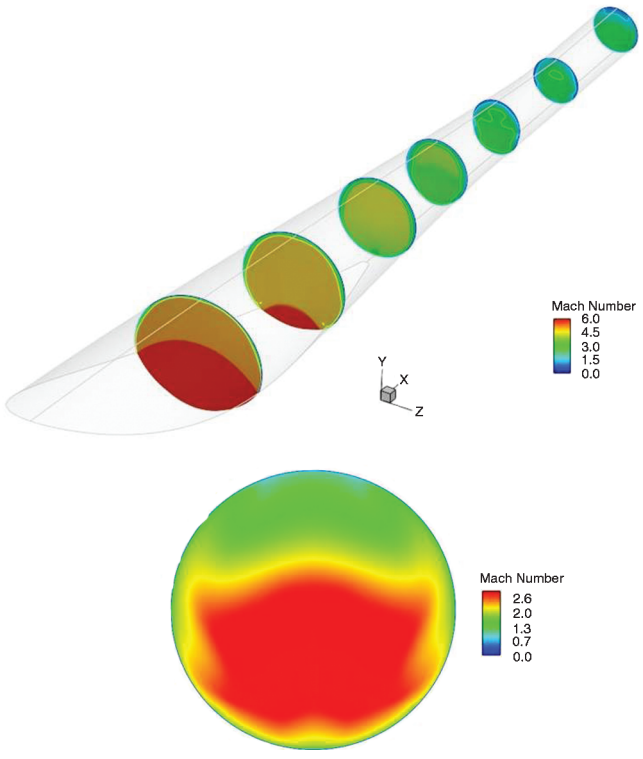

b) Scoop

Fig. 4 Mach number contours at symmetry, crossflow, and exit planes for Jaws and Scoop inlets.

2. Injection Configuration Development

The injector locations were derived from parametric studies on rectangular supersonic combustor configurations [18] and subsequently extended to circular designs [24]. For completeness, these studies are now summarized. Ten different configurations were examined with fuel injectors placed at different points inside and outside the cavity placed 1 diameter downstream of the combustor entrance. The results showed that the fuel distributions differed significantly from one another for the different injection strategies even though the penetration rate was generally similar. Of the 10 cases considered, the three most promising cases (designated in [18] as rectangular combustor cases 1, 4, and 9; see left column of Fig. 5a) were generalized to the circular geometry case by revolution about its axis [24]. To avoid confusion, these are redesignated as A, B, and C (right column of Fig. 5a). These circular configurations had the same entrance area, fuel momentum ratio, cavity length (L), and depth (D) cavity as the rectangular counterpart.

The injection scheme, as well as mixing factor performance for both rectangular and circular combustors, is shown in Fig. 5.

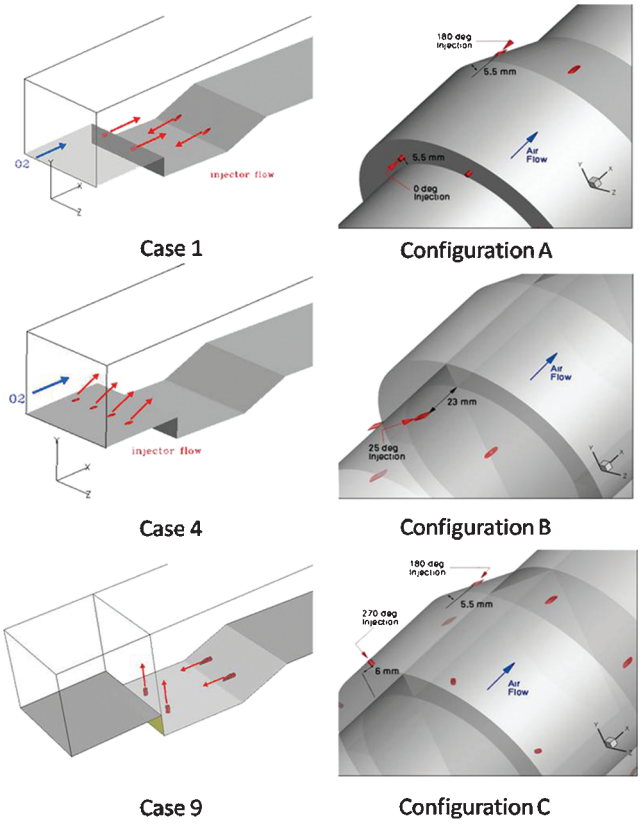

a) Injector configurations

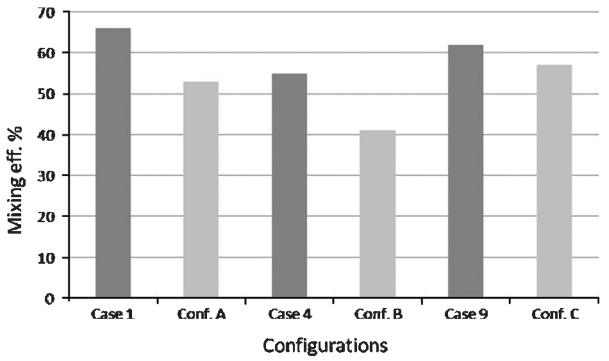

b) Mixing factor

Fig. 5 Configurations and mixing factor comparisons of combustors with frozen flow assumptions.

Although both frozen and finite rate chemistry are considered with uniform and distorted inflow profiles, only the frozen uniform cases are presented to illustrate the main points. Because it is difficult to distinguish mixing factor based on qualitative features, especially in nonchemically reacting flows, the mass fraction of C_2H_4 and O_2 distribution was integrated at the end of the exit plane to find the penetration or mixing factor for each case. The frozen mixing factor was measured by integrating gradients of species resulting from the fuel—air ratio over an ideal mixing value (premixed), as if these species were homogeneously distributed over the exit plane. For reacting cases, the combustion efficiency is defined by calculating fuel and oxygen consumed at the exit plane. For both frozen and reacting cases, fuel penetration distance was calculated at the closest point along the combustor core where the lower flammability limit of the fuel mass contours was obtained.

Based on previous studies [18,24], Fig. 5b shows that, for the rectangular arrangement, case 1 demonstrates the best performance, but configuration C (circular equivalent of case 9) is the best for the circular case. For the rectangular case 1, the fuel injector pattern helps drive the vortex inside the cavity continuously in its natural direction. Although the vertical penetration of the fuel in the rectangular case 4 was higher than the other two cases, its overall mixing factor was lower because, when the injectors are positioned upstream of the cavity (and angled at 25 deg), mixing in the spanwise direction is poor. Finally, results with C, which combines injection normal to the cavity floor and ramp, are similar to those with A. Even though the fuel penetration is similar to that with A, more dispersion in the crossflow direction was observed with C, due to normal injection at the bottom of the cavity. Overall, when comparing rectangular with circular geometries, the former configuration has superior performance (Fig. 5b). However, such a comparison should be qualified by the fact that the cavity volume for the circular case is larger than that for the rectangular case when assuming the same length and depth, rather than a constant ratio of these two. Figure 6 shows geometrical details for the study combustor configuration C.

Focusing now only on the circular cases, distortions due to shock–boundary-layer interactions in the Jaws inlet increase the mixing factor slightly, relative to the Scoop inlet. One possibility for the small difference is that the injection strategy does not take advantage of the vortical structure created by Jaws, and other arrangements may be superior in this case. In the previous study [24], a comparison of nonreacting cases showed that injection strategy C was the most efficient, again due to the first pair of injectors located at the front-bottom wall of the cavity and directed perpendicular to the air upstream.

The reacting cases confirm that configuration C resulted in greater fuel penetration than the other cases and stronger recirculation inside the cavity. Temperature and pressure, together with an air–fuel ratio at approximately ideal stoichiometric proportions in the cavity region, resulted in autoignition in this configuration. Injection strategies that drove the cavity vortex in its natural direction were again seen to be particularly beneficial. Based on these results [24], C was selected to further explore distortion effects of both inlets as well as model fidelity comparisons.

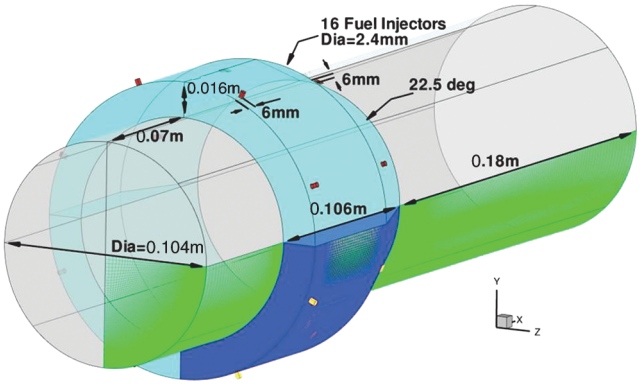

Fig. 6 Circular combustor for configuration C.

3. *Combustor Performance with Frozen Chemistry (Cases 1–3a)*

The Mach number and temperature contours for the uniform inflow case with frozen chemistry are shown in Figs. 7a and 7b, respectively. Each quantity is plotted in a 3-D view (top) to provide an overview of the flow distortion, whereas details are more clearly observed on the vertical (bottom, z-symmetry) plane. As noted earlier, the first set of injectors is positioned perpendicular to the airflow on the floor of the cavity. These jets affect the development of the shear layer, creating a greater compression in the core while expanding the recirculation region around the cavity. A small disk is formed on the centerline through the convergence of two sets of conical pressure waves. The first originates at the leading edge of the combustor, whereas the second arises due to the displacement of the cavity shear layer by the first injector set. The wave structure subsequently interacts with the rear of the cavity ramp and other locations downstream. The second set of injectors, positioned at the cavity ramp and facing toward the front wall, is intended to aid fuel–air mixture rotation in the natural counterclockwise direction. This

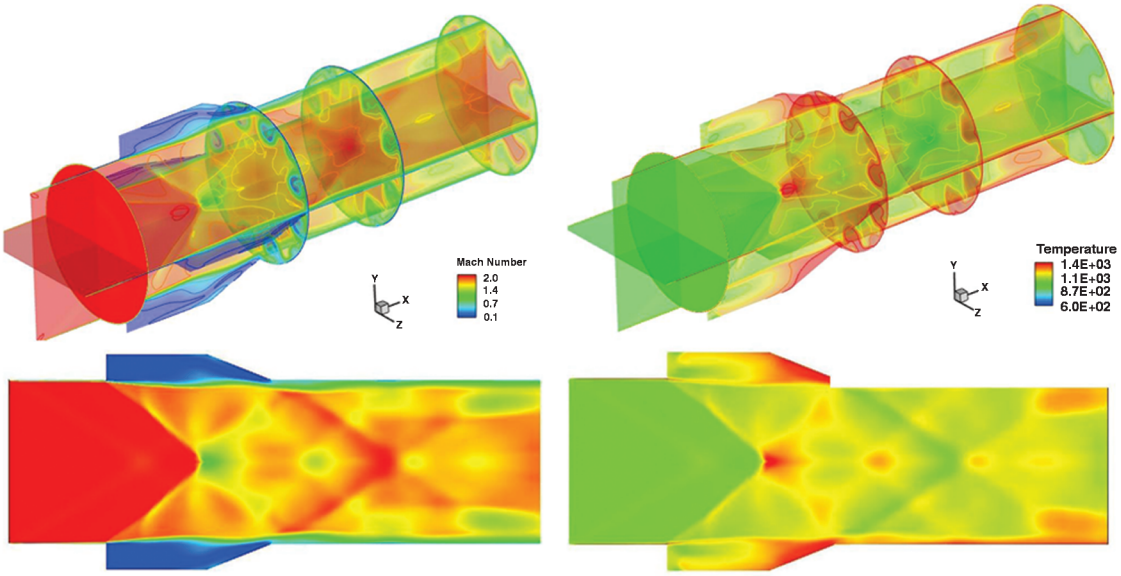

a) Mach number **b) Temperature**

Fig. 7 Three-dimensional (top) and symmetry plane (bottom) contours in combustor for frozen uniform inflow (case 1a).

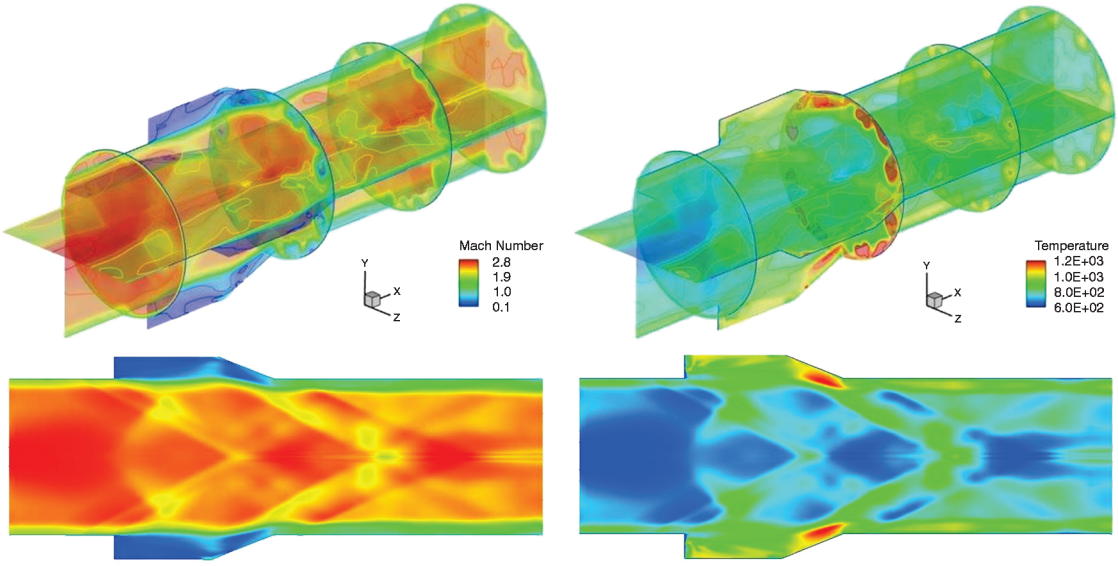

a) Mach number **b) Temperature**

Fig. 8 Three-dimensional (top) and symmetry plane (bottom) contours in combustor for frozen Jaws inflow (case 2a).

second set is not very effective because it lies in the shadow of the effects associated with the first set, consistent with previous observation [24]. The mixing factor is estimated to be 57% and the integrated Φ (equivalent fuel–air ratio) inside the cavity is about 1.0. The volume-averaged temperature and pressure inside the cavity are 1150 K and 0.15 MPa, respectively. Here the volume inside the cavity is estimated from the leading edge of the step to the leading edge of the ramp.

The Mach number and temperature contours (3-D view and at the combustor z-symmetry plane), assuming the Jaws inlet profile and frozen chemistry, are shown in Figs. 8a and 8b (case 2a). Again, the first set of injectors, positioned perpendicular to the airflow on the floor of the cavity, perturb the development of the shear layer. This creates similar effects as the previous case, with a greater compression at the core and expansion around the cavity. The disk formed on the centerline through the convergence of the shear layer displacement induced pressure waves is much smaller. The averaged Φ, temperature, and pressure inside the cavity volume reduce to 0.5, 970 K, and 0.09 MPa compared to the uniform inflow case. The Jaws profile develops a higher pressure in front of and inside the cavity where the first set of injectors are located. Although this larger pressure below the step (relative to the uniform case 1a) produces poorer fuel penetration and retains fuel closer to the walls compared to case 1a, the mixing factor increases to approximately 63%.

Figure 9 shows frozen chemistry results for the Scoop inflow (case 3a). As opposed to Jaws, the temperature is higher and pressure is lower near the end of the cavity ramp, allowing the fuel to travel further away from the walls. The Scoop profile generates a larger low-velocity region near the cavity (see bottom of Fig. 4b). The large deficit of momentum in the Scoop distorted profile also reflects higher temperatures near the lower surface. In this region (as opposed to the upper region), an augmented fuel penetration pattern is observed. Similarly, the uneven interactions of the shear and pressure waves yield an asymmetric contour map of the fuel dispersion inside the cavity. The mixing factor is estimated to be 60% whereas the averaged Φ, temperature, and pressure inside the cavity are 0.7, 971 K, and 0.1 MPa, respectively.

Figure 10 shows static pressure along the centerline of the combustor with frozen chemistry for the three inflow profiles (cases 1–3a). The uniform inflow shows a higher pressure spike because of the 3-D oblique shock interaction from the cavity leading edge. The

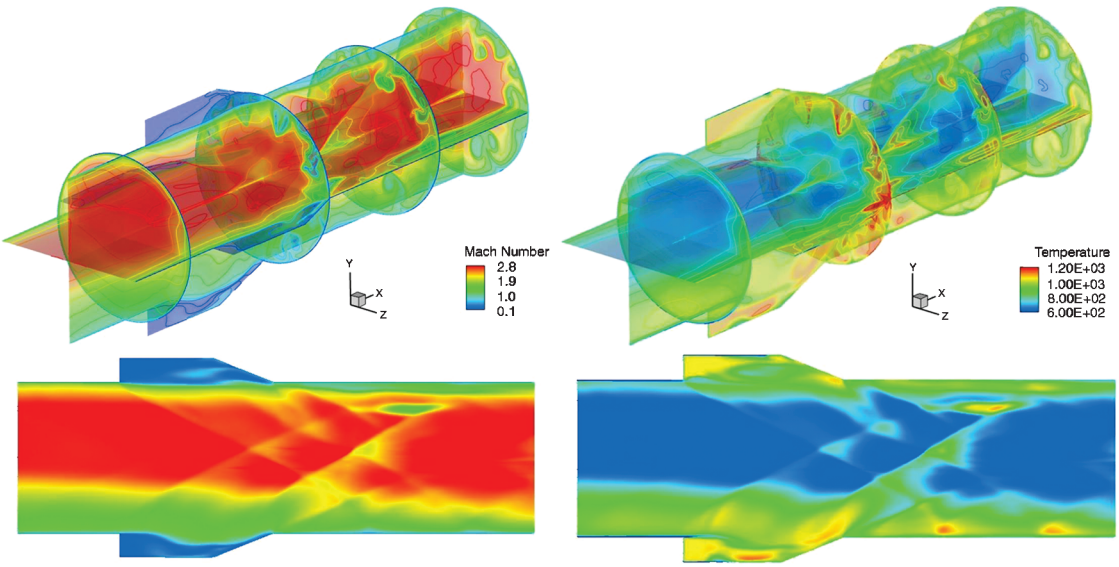

a) Mach number **b) Temperature**

Fig. 9 Three-dimensional (top) and symmetry plane (bottom) contours in combustor for frozen Scoop inflow (case 3a).

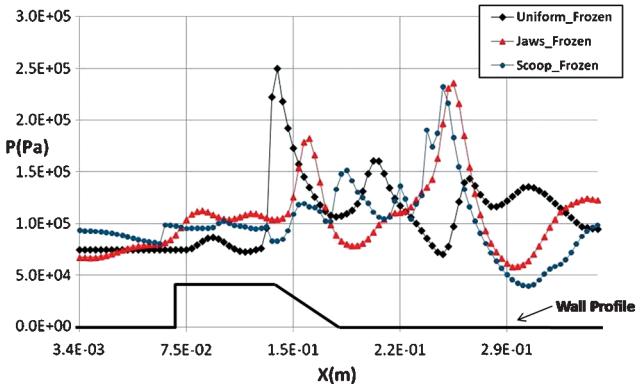

Fig. 10 Pressure along centerline for frozen flow with different inflow conditions (cases 1–3a).

Jaws and Scoop profiles produce higher pressure variation further downstream of the cavity ramp. Together with Figs. 8 and 9, the variation of inflow profile yields significantly different contraction and expansion patterns. The line plot and corresponding Mach number contours for the uniform case (Fig. 7) show that the flow across the cavity produces a series of pressure wave interactions in a diamond shape through the core. As the flow develops further downstream from the step, the pressure oscillations lessen and the field becomes more uniform. However, when comparing the pressure variations for the nonuniform cases (Jaws and Scoop), these nondesirable interactions increase past the cavity toward the exit of the combustor.

Thus, the comparison of Jaws and Scoop shows different flow patterns due to the characteristic distortion of each inlet with the cavity and subsequent interaction with the jets. The aforementioned variations in performance parameters suggest that further injection strategies need to be developed and explored to enhance the fuel penetration and exploit the incoming vortical structure in conjunction with modifications to cavity circulation.

4. *Combustor Performance with Chemistry (Cases 1–3b)*

The results obtained with finite rate chemistry for the uniform inflow conditions are shown in Fig. 11 (case 1b). Several conclusions are readily apparent when these figures are compared to equivalent results in the frozen cases. Both Mach number and temperature contours on the z-symmetry plane of the reacting case reveal a more pronounced high-compression disk-shaped area upstream of the cavity, which is absent in the frozen simulation. The results also indicate that chemical reactions are initiated upstream of the cavity, with fuel traveling upstream of the injector. The injection on the cavity floor and associated combustion pressure rise result in an earlier detachment of the cavity shear layer, even before the step. The reversed flow carries fuel and reaction products upstream of the cavity. In contrast to the nonreacting uniform case, the fuel mass fraction (Fig. 11, bottom left) shows enhanced diffusion within the cavity region, resulting in a combustion efficiency of about 64%. As previously anticipated from case 1a, this indicates a possibility of relatively rapid reactions due to the existence of high temperatures.

Figure 12 shows Mach number and temperature results obtained for the chemically reacting flow with the Jaws inflow condition (case 2b). In this case also, chemical reactions are observed upstream of the cavity. Considering the frozen (Fig. 8) versus reactive (Fig. 12) models for the Jaws inflow profile, the latter shows larger compression toward the center of the combustor due to the bowed shock. The shear-layer separation shows small upstream movement but is detached further from the wall. The variation in the boundary-layer profile upstream of the cavity indicates that the combustion pressure rise is positioned on the edge of the step, in front of the cavity. A larger region of low Mach number is observed inside the cavity, caused by the higher temperature and pressure produced by chemical reactions. The distorted incoming profile (see Fig. 4a) contains entrained high-speed fluid near the surface. This higher Mach number and distortion produced at the inlet mitigates further upstream fuel displacement and/or flashback effect relative to the uniform case (case 1b). Case 2b shows slightly superior fuel penetration and thicker shear-layer development near the cavity than case 2a. The average combustion efficiency calculated under this steady-state assumption reaches about 67%, marginally higher than the other circular cases. As computed from the inlet (see Fig. 12), stronger vortical structures are observed on the upper and lower regions with diminished shear on the sides. In addition, this interaction further disperses fuel from the cavity and aids combustion, as evident on the z-symmetry plane (see Mach number and temperature, Fig. 12 bottom left and right, respectively).

The results obtained for the Scoop inflow conditions assuming finite rate chemistry are shown in Fig. 13 (case 3b). An examination reveals significant differences from the Jaws solution. The Mach number and temperature contours on the z-symmetry plane of this reacting case indicate a three-dimensional oblique compression area upstream of the cavity. Its conical shape is distorted by the reduced-velocity region on the lower part (recall that the Scoop profile does not display symmetry about the horizontal plane), which positions the shock further upstream from the step than in the frozen Scoop

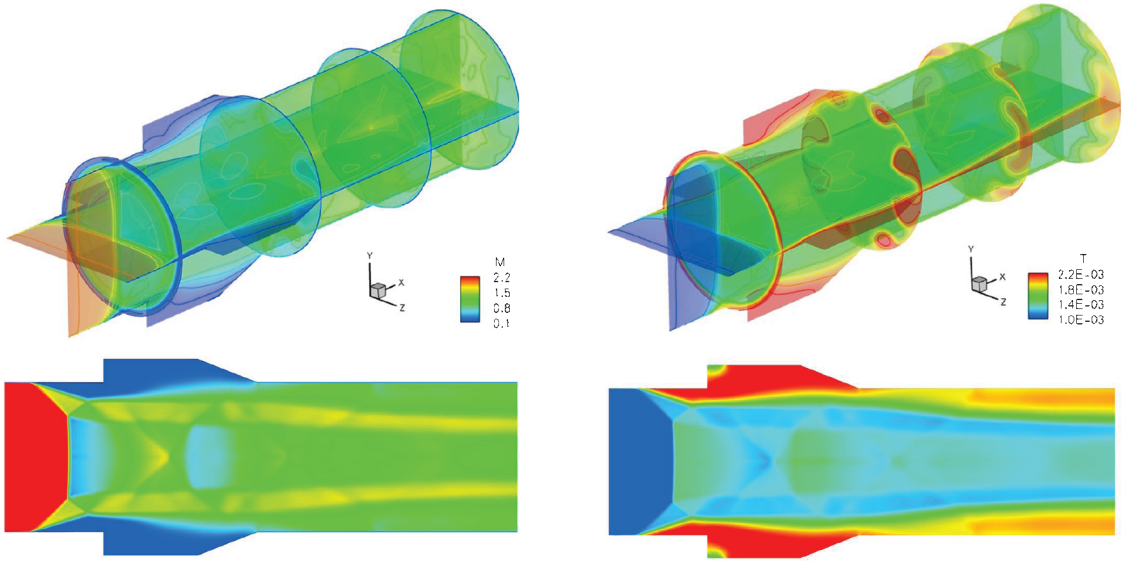

a) Mach number **b) Temperature**

Fig. 11 Three-dimensional (top) and symmetry plane (bottom) contours in combustor for reacting uniform inflow (case 1b).

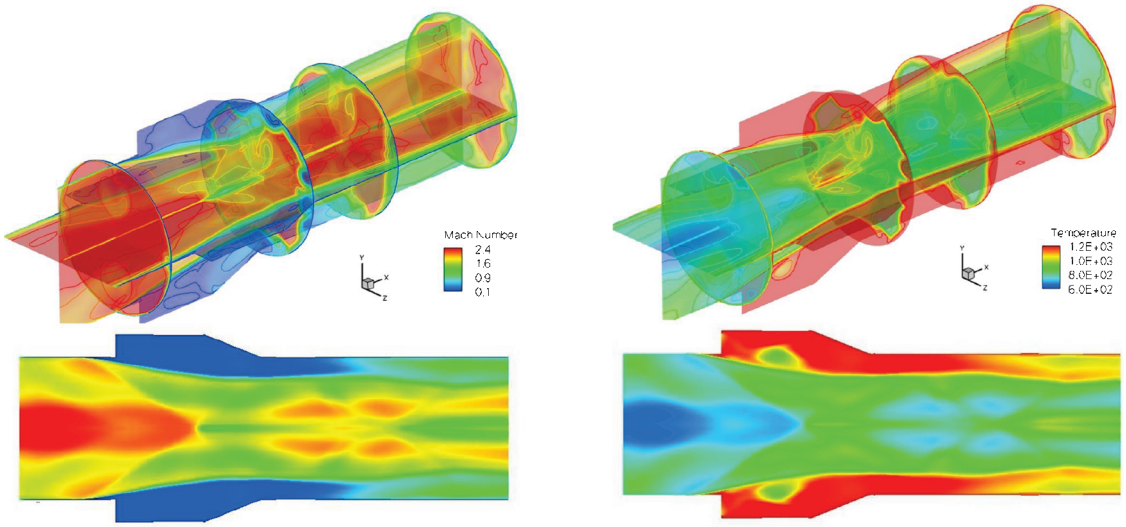

a) Mach number b) Temperature

Fig. 12 Three-dimensional (top) and symmetry plane (bottom) contours in combustor for reacting Jaws inflow (case 2b).

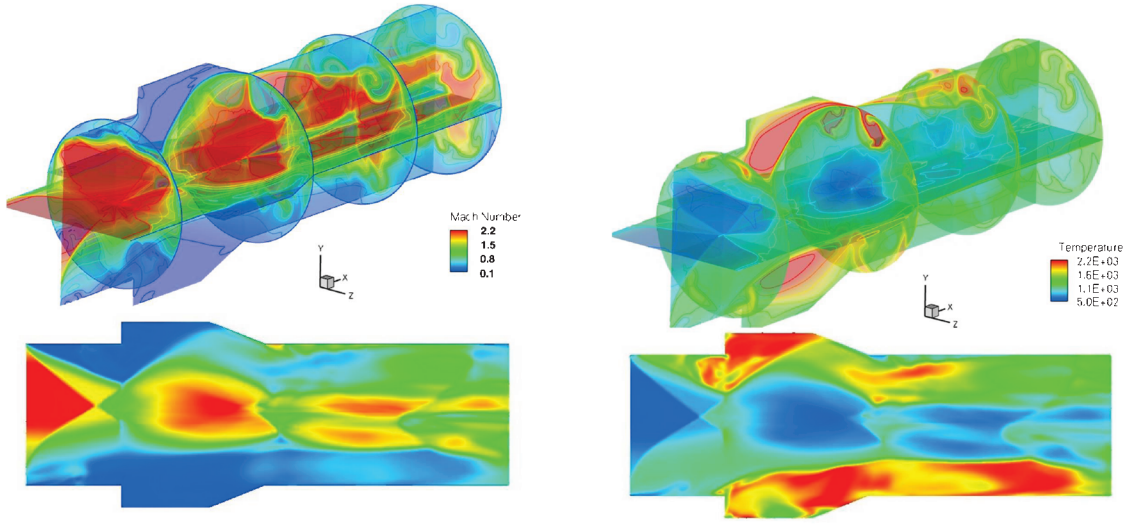

a) Mach number b) Temperature

Fig. 13 Three-dimensional (top) and symmetry plane (bottom) contours in combustor for reacting Scoop inflow (case 3b).

case (compare Figs. 9–13). The mechanism is similar to that observed for the uniform inflow cases previously studied [24], but specifics of the pattern are different because of the variation in the entrance profile. Scoop exhibits a larger circulation region ahead of the jet, further allowing the fuel to travel forward, affecting the area near the inflow boundary condition This indicates the potential for unstart and requires further analysis with a full tip-to-tail simulation. The average combustion efficiency for Scoop was about 63%.

The effect of reactions on centerline pressure is shown in Fig. 14 (cases 1–3b). Jaws results in a much higher combustion pressure, with peaks at the core of the combustor before the cavity ramp twice as high as with the uniform and the Scoop inflow. This is produced by a conical shock interaction that is stronger than in the other two cases (see Fig. 12a). When the Jaws inflow profile is simulated with chemistry, the pressure waves interacting across the cavity decay past the cavity and show smaller values downstream, in contrast to the frozen assumption (case 2a, shown in Fig. 10). On the other hand, the Scoop profile does not show much difference at the center relative to the uniform inflow case (see Fig. 13a). In this case, the lower momentum region at the bottom half of the Scoop inflow induces centerline pressure oscillations upstream.

A comparison of the effect of each inflow profile on reactive cases is summarized in Fig. 15, which shows CO radical mass fraction contours. These solutions indicate that the Jaws inlet profile can significantly lower the fuel–air ratio levels inside the cavity, helping push the fuel toward the core. In addition to fuel–air mixing, which correlates with combustion, the normalized integrated thrust per unit area ratio was also computed:

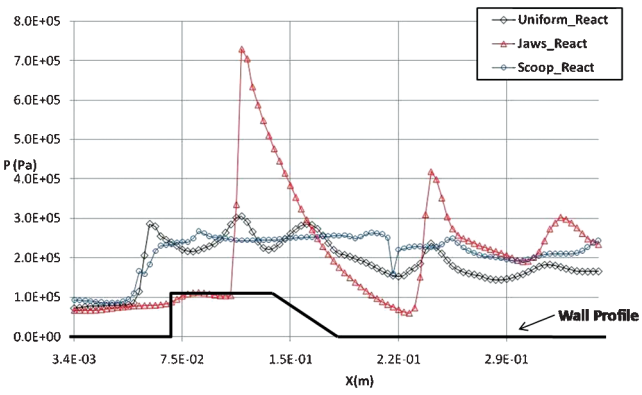

Fig. 14 Pressure along centerline flow with different inflow conditions (cases 1–3b).

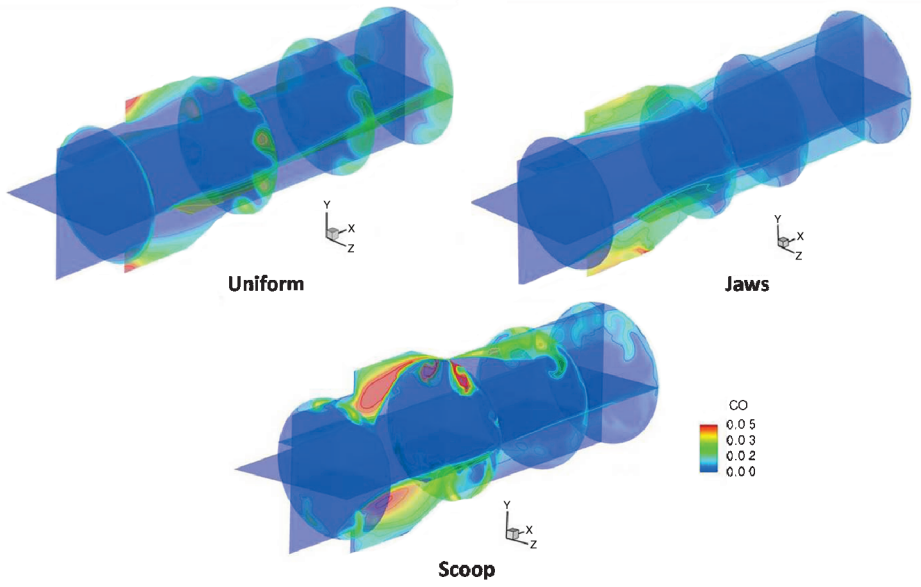

Fig. 15 Mass fraction CO contours at symmetry planes (cases 1–3b).

$$\Im = \int \frac{(\dot{m}_i + \dot{m}_f)u_e/A_i + P_e}{\dot{m}_i u_i/A_i + P_i}\partial A_i \tag{1}$$

where A is the cross-sectional area, P is the static pressure, and $\dot{m}$ is the mass flow rate. The subscripts f, i, and e refer to fuel, inlet (entrance), and exit boundary planes, respectively. The values for uniform Jaws and Scoop inflow profiles are 2.23, 2.63, and 2.22, respectively (see Table 3). These results are consistent with the expectation that fuel–air combustion efficiency increases correlate with thrust generation.

Although the motivation for these simulations is to understand the primary flow physics in the device, these configurations are relatively short and extend only a few cavity lengths downstream. For practical devices, the effects of combustor length (which is much larger) and associated flow and chemical time scales must be factored into the analysis.

B. Large Eddy Simulation versus Unsteady Reynolds Averaged Navier–Stokes: Averaged Inflow and Finite Rate Chemistry

As mentioned in Sec. II, these unsteady cases assume the uniform inflow condition and compute only a one-eighth circumferential

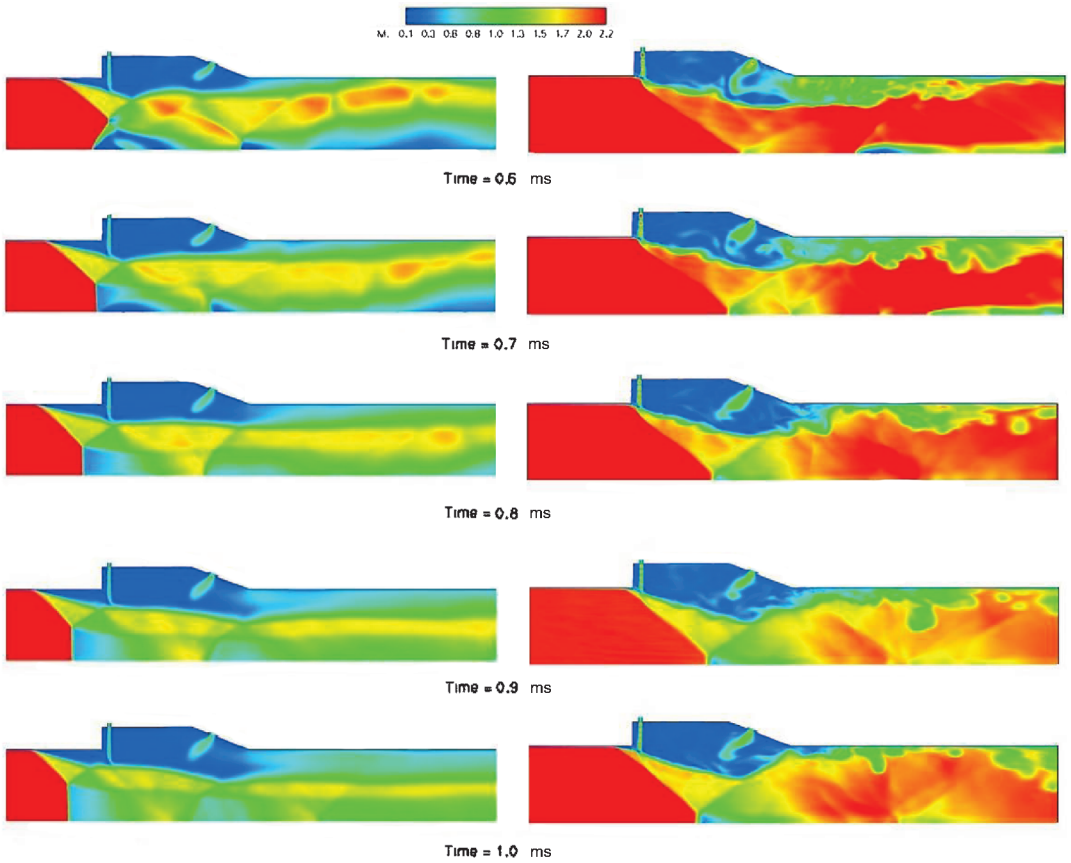

Fig. 16 Mach number contours with finite rate chemistry: URANS (left side) versus LES (right side).

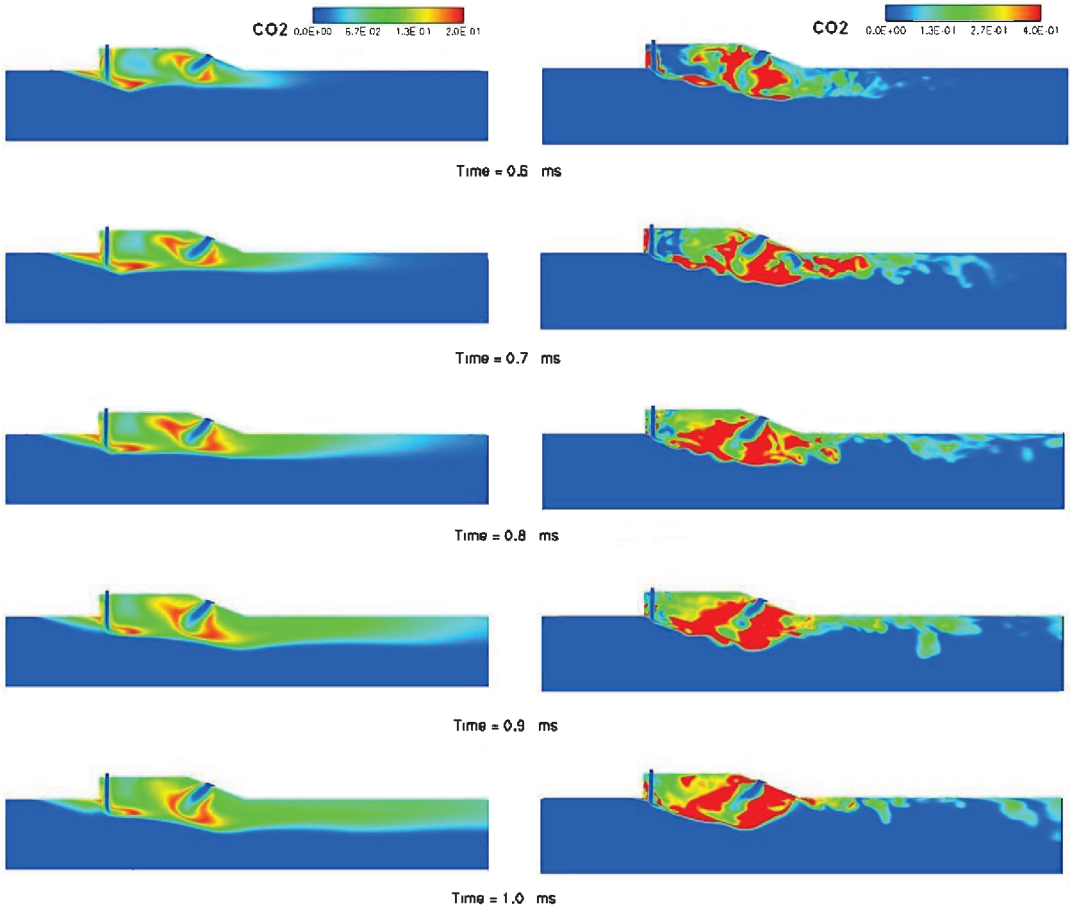

Fig. 17 Mass fraction product of CO_2 with finite rate chemistry: URANS (left side) versus LES (right side).

sector to minimize the computational effort. URANS (case 4) and LES (case 5) results for reacting chemistry at five time frames are compared in Fig. 16, at the azimuthal plane of the simulation that cuts through the fuel ports. An immediate and expected observation is that the LES result shows the development of small scales, whereas the URANS result does not. URANS shows a larger combusting region upstream of the cavity backstep. The initial conical shock arising from the reaction terminates in a normal (unsteady) shock, similar to that observed in an irregular reflection. However, with reactive URANS, the normal upstream shock results in the entire subsequent region being subsonic, and though some small scale structures are evident in the initial development (see frame for 0.6 ms), these details subsequently diminish. Solution evolution can eventually result in essentially an unstartlike scenario, in which the disturbance reaches the upstream boundary. In contrast, the LES result shows a considerably smaller upstream reaction region and a series of weak oblique shocks. These results are consistent with lower fuel mixing and combustion in the cavity than for URANS.

LES predicts higher fuel-air mixing and combustion in the cavity than URANS, confirming that the resolution of the details of the different processes inside the cavity have a significant impact on the overall flow development and promotion of chemical reactions. These observations are reinforced by examination of the CO_2 contours shown in Fig. 17. The combustion regions with the two models are vastly different, with URANS being considerably smeared relative to the LES case. Note in this context, to highlight differences and elucidate the structure, the scales for the two cases are different for the CO_2 contours, with the LES scale spanning twice the range of the URANS. The fuel path is evident in both sets of calculations. However, the LES jet shows a more detailed structure in which the air fuel interaction is initiated much earlier; note the large differences in product formed even at 0.6 ms. In this context, the two approaches (LES and URANS) are obtained from very different theoretical considerations (Reynolds averaging versus spatial filtering). Thus, caution must be exercised in making direct comparisons of structure size. Whereas the URANS simulation shows a demarcation between the reactants formed by the first and second sets of fuel injectors along the cavity wall, the LES combustion domain shows flow fluctuations along the cavity and main duct stream. The effect of the lifting of the shear layer, associated with the first set of injectors, facilitates a greater region of combustion associated with the second set. At the last time frame plotted, the URANS result shows a relatively constant combustion region height from the cavity walls, whereas the products in the LES simulation show flow fluctuations along the transverse and vertical directions, due to cavity separation. This leads to more fuel penetration at the combustor exit and a larger recirculation zone in the cavity region with a low Mach number, as shown in Fig. 16. By comparing the average injected fuel to the burned mole fraction values at the exit over the selected time (2 ms from the assumed ignition time), the combustion efficiency is higher for LES by approximately 8% compared to URANS.

IV. Conclusions

The effect of a uniform or actual distorted inflow profile (either by a Jaws or a Scoop inlet) on a supersonic combustor has been explored with frozen as well as finite rate kinetics under steady and unsteady state assumptions. The results show strong sensitivity in terms of performance characteristics and flow structures. Overall, the Jaws inflow profile demonstrates higher values of mixing, combustion efficiency, and thrust ratio because of its greater distortion pattern. The results suggest that the fuel injection strategy may be further optimized to take advantage of the features present at the exit of each inlet. Chemical reactions do not affect the trends but do yield different efficiencies and strengths of flow features. Unlike at frozen conditions, a high-compression region appears upstream of the cavity, which impacts the development of the shear layers and downstream combustion. URANS and LES calculations are used to study both

turbulent approaches and determine directions for further detailed analysis for cavity stability and volume effects. Comparing URANS with LES, the former does not resolve the small structures and displays overall higher diffusion, which translates into large scale differences in flow structure. For example, the reacting shock structure propagates significantly more upstream with URANS. The chemical reaction time is observed to be lower in URANS than LES, possibly due to the higher diffusion in RANS. This reduces the ignition time and, therefore, results in a higher Damköhler number. Although the LES results in a larger recirculation region in the cavity, the transient shock structure is weaker. This work is currently being extended to full tip-to-tail analyses, to explore the effect of upstream influence of the combustor on inlet performance.

Acknowledgments

The authors are grateful to U.S. Air Force Office of Scientific Research for supporting this work (monitors: J. Schmisseur and F. Fahroo) and to the Department of Defense High Performance Computing Modernization Program for computational resources through the Major Shared Resource Centers at U.S. Air Force Research Laboratory and Naval Oceanographic Office. The Scoop inlet geometry is based on a design provided by G. Candler (University of Minnesota), modified to remove leading-edge details to provide a simpler mesh topology.

References

[1] Curran, E., and Murthy, S., *Scramjet Propulsion*, Vol. 189, Progress in Aeronautics and Astronautics, AIAA, Reston, VA, 2001.

[2] Walker, S., Rodgers, F., and Esposita, A., "Hypersonic Collaborative Australia/United States Experiment (HYCAUSE)," AIAA Paper 2005-3254, 2005.

[3] Billig, F., and Jacobsen, L., "Comparison of Planar and Axisymmetric Flowpaths for Hydrogen Fueled Space Access Vehicles (Invited)," AIAA Paper 2003-4407, 2003.

[4] Drayna, T., Nompelis, I., and Candler, G., "Hypersonic Inward Turning Inlets: Design and Optimization," AIAA Paper 2006-297, Jan. 2006.

[5] Ungewitter, R., Ott, J., and Dash, S., "Advanced Modeling Methods for Hypersonic Scramjet Evaluation," AIAA Paper 2006-4578, 2006.

[6] Menon, S., and Patel, N., "Subgrid Modeling for Simulation of Spray Combustion in Large-Scale Combustors," *AIAA Journal*, Vol. 44, No. 4, 2006, pp. 709–723. doi:10.2514/1.14875

[7] Gicquel, L., Givi, P., Jaberi, F., and Pope, S., "Velocity Filtered Density Function for Large Eddy Simulation of Turbulent Flows," *Physics of Fluids*, Vol. 15, No. 8, 2003, pp. 2321–2337. doi:10.1063/1.1584678

[8] Ebrahimi, H., "Numerical Investigation of Jet Interaction in a Supersonic Freestream," *Journal of Spacecraft and Rockets*, Vol. 45, No. 1, 2008, pp. 95–103. doi:10.2514/1.29847

[9] Malo-Molina, F., Gaitonde, D., and Kutschenreuter, P., "Numerical Investigation of an Innovative Inward Turning Inlet," AIAA Paper 2005-4871, June 2005.

[10] Tam, C.-J., and Baurle, R., "Inviscid CFD Analysis of Streamline Traced Hypersonic Inlets at Off-Design Conditions," AIAA Paper 2001-0675, 2001.

[11] Gaitonde, D., Malo-Molina, F., Croker, B., and Ebrahimi, H., "The Flowfield Structure in Generic Inward- Turning-Based Propulsion Flowpath Components," AIAA Paper 2007-5744, 2007.

[12] Goyne, C. E., McDaniel, J. C., Quagliaroli, T. M., Krauss, R. H., and Day, S. W., "Dual-Mode Combustion of Hydrogen in a Mach 5 Continuous-Flow Facility," *Journal of Propulsion and Power*, Vol. 17, No. 6, 2001, pp. 1313–1318. doi:10.2514/2.5880

[13] Ebrahimi, H., "Numerical Simulation of Transient Jet-Interaction Phenomenology in a Supersonic Freestream," *Journal of Spacecraft and Rockets*, Vol. 37, No. 6, 2000, pp. 713–719. doi:10.2514/2.3634

[14] Gruber, M., Jackson, K., Jackson, T., and Mathur, T., "Investigations of Shock Trains in Rectangular Ducts," JANNAF Paper 4D-03, Dec. 1998.

[15] Mathur, T., Lin, K.-C., Kennedy, P. J., Gruber, M. R., Donbar, J. M., Jackson, T. A., and Billig, F., "Liquid JP-7 Combustion in a Scramjet Combustor," AIAA 2000-3581, July 2000.

[16] Berman, H., Anderson, J. D., J., and Drumond, J., "Supersonic Flow over a Rearward Facing Step with Transverse Nonreacting Hydrogen Injection," *AIAA Journal*, Vol. 21, No. 12, 1983, pp. 1707–1713. doi:10.2514/3.8313

[17] Kim, K., Baek, S., and Han, C., "Numerical Study on Supersonic Combustion with Cavity-Based Fuel Injection," *International Journal of Heat and Mass Transfer*, Vol. 47, No. 2, 2004, pp. 271–286. doi:10.1016/j.ijheatmasstransfer.2003.07.004

[18] Ebrahimi, H., Gaitonde, D., and Malo-Molina, F., "Parametric Study of 3-D Hydrocarbon Scramjet Engine with Cavity," AIAA Paper 2007-0645, Jan. 2007.

[19] Gruber, M., Jackson, K., Mathur, T., and Billig, F., "Experiments with a Cavity-Based Fuel Injector for Scramjet Application," International Society of Air-Breathing Engines, Paper IS-7154, Sept. 1999.

[20] Baurle, R., Tam, C.-J., and Dasgupta, S., "Analysis of Unsteady Cavity Flows for Scramjet Applications," AIAA Paper 2000-3617, 2000.

[21] Ben-Yakar, A., and Hanson, R., "Cavity Flame-Holders for Ignition and Flame Stabilization in Scramjets: An Overview," *Journal of Propulsion and Power*, Vol. 17, No. 4, 2001, pp. 869–877. doi:10.2514/2.5818

[22] Gruber, M., Baurle, R., Mathur, T., and Hsu, K.-Y., "Fundamental Studies of Cavity-Based Flame Holder Concepts for Supersonic Combustors," *Journal of Propulsion and Power*, Vol. 17, No. 1, 2001, pp. 146–153. doi:10.2514/2.5720

[23] Baysal, O., and Stallings, R., "Computational and Experimental Investigation of Cavity Flow Fields," *AIAA Journal*, Vol. 26, No. 1, 1988, pp. 6–7. doi:10.2514/3.9842

[24] Malo-Molina, F., Gaitonde, D., Ebrahimi, H., and Ruffin, S., "Scramjet Combustor Analysis Integrated to an Innovative Inward Turning Inlet," AIAA Paper 2008-4577, 2008.

[25] Wilcox, D., "Turbulence Modeling—An Overview," AIAA Paper 2001-0724, 2001.

[26] Kim, W., and Menon, S., "Application of the Localized Dynamic Subgrid-Scale Model to Turbulent Wall- Bounded Flows," AIAA Paper 97-0210, 1997.

[27] Schluter, J., and Pope, S., "Large-Eddy Simulation Inflow Conditions for Coupling with Reynolds-Averaged Flow Solvers," *AIAA Journal*, Vol. 42, No. 3, 2004, pp. 478–484. doi:10.2514/1.3488

[28] Ebrahimi, H., "Validation Database for Propulsion Computational Fluid Dynamics," *Journal of Spacecraft and Rockets*, Vol. 34, No. 5, 1997, pp. 642–649. doi:10.2514/2.3262

[29] Ebrahimi, H., "An Overview of Computational Fluid Dynamics for Application to Advanced Propulsion Systems," AIAA Paper 2004-2370, 2004.

[30] Zhou, X. Y., and Pereira, J. C. F., "Large Eddy Simulation of a Reacting Plane Mixing Layer Using Filtered Density Function," *Flow, Turbulence and Combustion*, Vol. 64, 2000, pp. 279–300. doi:10.1023/A:1026595626129

[31] Raman, V., Cook, D., and Pitsch, H., "Hybrid LES/FDF Simulation of a Non-Premixed Bluff-Body Stabilized Flame," *Bulletin of the American Physical Society*, Vol. 49, No. 9, 2004, pp. 57–58.

[32] Glaze, D. J., Frankel, S. H., and Hewson, J. C., "Non-Premixed Turbulent Jet Mixing Using LES with the FMDF Model," *30th International Symposium on Combustion, Abstracts of Work-In-Progress Posters*, Combustion Inst., Pittsburgh, PA, 2004.

[33] Lu, L., Ren, Z., Raman, V., Pope, S. B., and Pitsch, H., "LES/FDF/ISAT. Computations of Turbulent Flames," *Proceedings of the 2004 Summer Program, Center for Turbulence Research*, NASA Ames Research Center/Stanford Univ., Stanford, CA, 2004, pp. 283–294.

[34] Dixon-Lewis, G., *Complex Chemical Reaction Systems*, Springer–Verlag, Berlin, 1987, pp. 47–265.

[35] Gaitonde, D., and Shang, J., "On 3-D Shock-Wave/Turbulent Boundary Layer Interactions at Mach 4," AIAA Paper 96-0043, Jan. 1996.

F. Ladeinde
Associate Editor